Published in final edited form as:
Neuroimage. 2014 January 15; 85(0 1): . doi:10.1016/j.neuroimage.2013.01.073.

Further improvement in reducing superficial contamination in NIRS using double short separation measurements

Louis Gagnon[a,b], **Meryem A. Yücel**[a], **David A. Boas**[a,b], and **Robert J. Cooper**[a,c]

[a]Athinoula A. Martinos Center for Biomedical Imaging, Department of Radiology, Massachusetts General Hospital, Harvard Medical School, Charlestown, MA, USA

[b]Harvard-MIT Division of Health Sciences and Technology, Cambridge, MA, USA

[c]Department of Medical Physics and Bioengineering, University College London, London, UK

Abstract

Near-Infrared Spectroscopy (NIRS) allows the recovery of the evoked hemodynamic response to brain activation. In adult human populations, the NIRS signal is strongly contaminated by systemic interference occurring in the superficial layers of the head. An approach to overcome this difficulty is to use additional NIRS measurements with short optode separations to measure the systemic hemodynamic fluctuations occurring in the superficial layers. These measurements can then be used as regressors in the post-experiment analysis to remove the systemic contamination and isolate the brain signal. In our previous work, we showed that the systemic interference measured in NIRS is heterogeneous across the surface of the scalp. As a consequence, the short separation measurement used in the regression procedure must be located close to the standard NIRS channel from which the evoked hemodynamic response of the brain is to be recovered. Here, we demonstrate that using two short separation measurements, one at the source optode and one at the detector optode, further increases the performance of the short separation regression method compared to using a single short separation measurement. While a single short separation channel produces an average reduction in noise of 33% for HbO, using a short separation channel at both source and detector reduces noise by 59% compared to the standard method using a general linear model (GLM) without short separation. For HbR, noise reduction of 3% is achieved using a single short separation and this number goes to 47% when two short separations are used. Our work emphasizes the importance of integrating short separation measurements both at the source and at the detector optode of the standard channels from which the hemodynamic response is to be recovered. While the implementation of short separation sources presents some difficulties experimentally, the improvement in noise reduction is significant enough to justify the practical challenges.

Keywords

Near-Infrared Spectroscopy; Systemic Interference; Short Optode Separations; Kalman filtering; State-Space analysis

1. Introduction

Near-Infrared Spectroscopy (NIRS) is a non-invasive neuro-investigatory technique used to measure the hemodynamic changes associated with evoked brain activity (Obrig and Villringer, 2003; Hoshi, 2007; Lloyd-Fox et al., 2010; Ferrari and Caresima, 2012). In adult populations, the majority of functional NIRS studies are performed using a back-reflection geometry, with near-infrared light carried to and from the head via optical fibers. This back-reflection geometry ensures that the NIRS signal is extremely vulnerable to contamination by the hemodynamics within the superficial layers of the head.

It has recently been shown that this interference can be significantly reduced with the use of short separation (SS) recordings which are sensitive to superficial layers only, including the scalp and the skull (Saager and Berger, 2005; Zhang et al., 2007; Umeyama and Yamada, 2009). These SS measurements are used as regressors during the post-processing of the NIRS signal and have been shown to improve the detection of evoked brain activity using NIRS (Zhang et al., 2009; Saager et al., 2011; Yamada et al., 2009; Gagnon et al., 2011).

In our previous work (Gagnon et al., 2012), we showed that the superfical NIRS signal obtained by SS channels is spatially inhomogeneous across the scalp. In order to successfully regress the superficial signal from that of the brain, the SS measurement must therefore be located as close as possible to the long separation (LS) NIRS channel. For NIRS measurements performed on adult humans, the source and detector optodes are generally separated by around 3 cm, which is large enough to observe the hemodynamics of the cortex but short enough that enough light returns to the detector (Boas et al., 2004). Any change measured by a standard NIRS channel is the result of an integration of all optical changes which occur throughout the volume of tissue traversed by the NIR light. The NIRS signal will therefore invariably contain superficial interference from two different locations: beneath the source optode and beneath the detector optode and these interference signals may not correlate with one another. As a result, it is reasonable to hypothesize that the performance of the SS regression method will improve if the superficial NIRS signal is independently recorded from both the tissue beneath the source optode and from the tissue beneath the detector optode.

In this work, we investigated the performance of using two such SS measurements to regress systemic physiological signals from NIRS data.

2. Methods

2.1. Experimental measurements

Five healthy adult subjects were recruited for this study. The Massachusetts General Hospital Institutional Review Board approved the study and all subjects gave written informed consent. Data were collected using a TechEn CW6 system operating at 690 and 830 nm. The NIRS probe contained 8 sources and 8 detectors as shown in Fig. 1. The probe was designed to contain a SS measurement at each source and at each detector optode of the LS measurement to provide maximal overlap between the LS and the SS measurements. In order to avoid detector saturation, 200 μm-core fibers were used for the SS detectors (shown in red in Fig. 1) and an optical filter (Kodak WRATTEN ND 2.00) was glued to the tip of standard NIRS fiber bundles (shown in green in Fig. 1) for the additional sources of the SS measurements. The probe was secured over the left motor region of each subject.

During the experiment, subjects were sitting in a comfortable chair in front of a computer screen with a black background. The 6-minute long functional runs consisted of stimulus trials of 5-seconds of a finger tapping task, with an inter-trial interval varying randomly

between 12 and 18 sec. Each functional run contained between 19 and 21 trials and three functional runs were acquired for each subject. Between stimulus periods, a small 0.5-by-0.5 cm white square appeared at the center of the computer screen and the subjects were asked to fixate on this square. During the finger tapping periods, the instruction tap your fingers was displayed in white characters on the computer screen using the Psychophysics toolbox in Matlab (Brainard, 1997). The finger tapping task required the subject to touch their right thumb to each finger of their right hand in order as quickly as possible and repeat the process until the instruction left the computer screen. Following the three functional runs, three baseline runs of 5 minutes each were acquired. During the baseline runs, the subjects were asked to simply close their eyes and remain still.

2.2. Data analysis

An overview of the data analysis procedure is shown in Fig. 2. Both the SS and LS measurements were bandpass filtered at 0.01-1.25 Hz and then used simultaneously in a Kalman filter. The Kalman filter was identical to that described in our previous papers (Gagnon et al., 2011, 2012) with the addition of a second short separation regressor.

The hemodynamic response was modeled by

$$h[n] = \sum_{i=1}^{N_w} w_i b_i[n] \quad (1)$$

where $b_i[n]$ are normalized Gaussian functions with a standard deviation of 0.5 s and their means separated by 0.5 s. N_w is the number of Gaussian functions used to model the hemodynamic response and was set to 15 for our simulations to recover the HRF over 0-8 sec. The signal in the LS channel $y_{LS}[n]$ was modelled by a linear combination of the two SS signals $y_{SS}^{Src}[n]$ and $y_{SS}^{Det}[n]$ and the brain response $y_b[n]$. The expression for the LS signal is given by

$$y_{LS}[n] = y_b[n] + a_{Src} \quad y_{SS}^{Src}[n] + a_{Det} \quad y_{SS}^{Det}[n] \quad (2)$$

with

$$y_b[n] = \sum_{k=-\infty}^{\infty} h[k]\, u[n-k] \quad (3)$$

and where $u[n]$ is the onset vector which is a binary vector taking the value 1 when n corresponds to a time when the stimulus was presented and 0 otherwise. It is to note that $u[n]$ is equal to 1 only at the onset of the stimulus and not throughout the duration of the stimulus.

The variables a_{Src} and a_{Det} are the dynamic weights used to model the superficial signals in the LS separation channel as a linear combination of the two SS signals. Only a single time delay was taken from the short separation channels to model the superficial signals in the LS channel since this has been shown to result in a better performance in our previous paper (Gagnon et al., 2011). The states to be estimated by the Kalman filter were the weights of the superficial contribution a_{Src} and a_{Det} and the weights of the temporal bases w_i. All these weights were assumed to be time-varying. Eqs. (1), (2) and (3) can be re-written in state-space form:

$$\mathbf{x}[n+1] = \mathbf{I}\mathbf{x}[n] + \mathbf{w}[n] \quad (4)$$

$$y_{LS}[n] = \mathbf{C}[n]\,\mathbf{x}[n] + \mathbf{v}[n] \quad (5)$$

where **w**[*n*] and **v**[*n*] are the process and the measurement noise respectively. **x**[*n*] is the n^{th} instance of **x** given by

$$\mathbf{x} = \begin{bmatrix} w_1 & \cdots & w_{N_w} & a_{Src} & a_{Det} \end{bmatrix}^T. \quad (6)$$

The quantity **I** is an N_w + 2 by N_w + 2 identity matrix and **C**[*n*] is a 1 by N_w + 2 vector given by

$$\mathbf{C}[n] = \begin{bmatrix} u * b_1[n] & \ldots & u * b_{N_w}[n] & y_{SS}^{Src}[n] & y_{SS}^{Det}[n] \end{bmatrix}. \quad (7)$$

where "*" denotes the convolution operator. The estimate $\hat{\mathbf{x}}[n]$ at each sample *n* is then computed using the Kalman filter (Kalman, 1960) followed by the Rauch–Tung–Striebel smoother (Rauch et al., 1965).

The convergence of the Kalman filter depends on the initial estimate of the state vector $\hat{\mathbf{x}}[0]$. To overcome this problem, $\hat{\mathbf{x}}[0]$ was set to the values obtained using a static least-squares estimator as in (Gagnon et al., 2011) to ensure a fast convergence. Moreover, to overcome the problem of selecting a good initial guess for the state covariance estimate $\hat{\mathbf{P}}[0]$, the Kalman filter algorithm was run twice and the initial covariance estimate for the second run was set to the final covariance estimate of the first run. This process makes the performance of the filter almost insensitive to the initial covariance estimate. For the first pass of the Kalman filter, we set $\hat{\mathbf{P}}[0]$ to an identity matrix with diagonal entries of 1×10^{-1} for the temporal basis states and 5×10^{-4} for the superficial contribution state. The process noise covariance Q only contained nonzero terms on the diagonal elements. Those diagonal terms were set to 2.5×10^{-6} for the temporal basis states and 5×10^{-6} for the superficial contribution state. The measurement noise covariance **R** was set to an identity matrix scaled by 5×10^{-2}. These values were extensively studied in our previous paper (Gagnon et al., 2011) and multiplying or dividing these values by factor of 10 did not significantly a ect the performance of our method. The Kalman filter algorithm was then processed with the following prediction-correction recursion (Gelb, 1974):

$$\hat{\mathbf{x}}[n|n-1] = \hat{\mathbf{x}}[n-1|n-1] \quad (8)$$

$$\hat{\mathbf{P}}[n|n-1] = \hat{\mathbf{P}}[n-1|n-1] + \mathbf{Q}. \quad (9)$$

$$\mathbf{K}[n] = \hat{\mathbf{P}}[n|n-1]\,\mathbf{C}[n]^T \left(\mathbf{C}[n]\,\hat{\mathbf{P}}[n|n-1]\,\mathbf{C}[n]^T + \mathbf{R}\right)^{-1} \quad (10)$$

$$\hat{\mathbf{x}}[n|n] = \hat{\mathbf{x}}[n|n-1] + \mathbf{K}[n]\left(y_{LS}[n] - \mathbf{C}[n]\,\hat{\mathbf{x}}[n|n-1]\right) \quad (11)$$

$$\hat{\mathbf{P}}[n|n] = (\mathbf{I} - \mathbf{K}[n]\,\mathbf{C}[n])\,\hat{\mathbf{P}}[n|n-1]. \quad (12)$$

After the Kalman algorithm was applied twice, the Rauch–Tung–Striebel smoother was applied in the backward direction (Haykin, 2001):

$$\hat{\mathbf{x}}[n|N_t] = \hat{\mathbf{x}}[n|n] + \hat{P}[n|n]\,\hat{\mathbf{P}}[n+1|n]^{-1}\left(\hat{\mathbf{x}}[n+1|N_t] - \hat{\mathbf{x}}[n+1|n]\right) \quad (13)$$

with N_t the number of time points in the data. The complete time course of the filtered brain signal $\hat{y}_b[n]$ containing the estimated hemodynamic response $\hat{h}[n]$ was then reconstructed for each sample time n using the first N_w final state estimates $\hat{\mathbf{x}_b} = [w_1 \cdots w_{N_w}]^T$ and the temporal basis set contained in $\mathbf{C}[n]$

$$\hat{y}_b[n] = \mathbf{C}[n]\,\hat{\mathbf{x}}_b[n|N_t]. \quad (14)$$

This reconstructed filtered brain signal time course $\hat{y}_b[n]$ was further low pass filtered at 0.5 Hz to remove any cardiac fluctuations potentially present in the time course and the final estimate of the hemodynamic response $\hat{h}[n]$ was obtained by applying a standard General Linear Model (GLM) procedure (without any cosine bases or short separation regressor) containing the same temporal basis function as in Eq. (1). More details of the algorithm and the parameters used can be found in our previous papers (Gagnon et al., 2011, 2012).

2.3. Simulations

Simulations were performed as described previously (Gagnon et al., 2011, 2012) by adding a synthetic HRF to the three baseline NIRS recordings acquired in each subject. For each baseline measurement, the changes in optical density were converted to changes in hemoglobin concentrations using the modified Beer-Lambert relationship (Deply et al., 1988). A pathlength correction factor of 6 and a partial volume correction factor of 50 were applied (Strangman et al., 2003; Huppert et al., 2006a,b).

An overview of the simulation procedure is shown in Fig. 3. Thirty individual simulated evoked responses were added over each of the 60 LS channel baseline measurements (5 subjects × 3 runs × 4 LS channels), with randomized onset times such that the inter-stimulus intervals varied between 12 and 30 seconds.

There is increasing evidence that many functional activation tasks give rise to systemic changes in oxyhemoglobin concentration which are time locked to the stimulus (Kirilina et al., 2011; Takahashi et al., 2011). These evoked systemic signals are likely due to an increase in heart rate and blood pressure associated with the performance of a task. We therefore added an evoked systemic artifact that was phase-locked with the stimulus to better represent real functional experiments. The artifact was added to both the LS and SS HbO signals. We used a sinusoidal function to model the artifact and the phase was chosen such that the peak of the artifact matches the peak of the hemodynamic response. No artifacts were added to the HbR traces since no evoked systemic artifacts have been reported for HbR signals (Kirilina et al., 2011; Takahashi et al., 2011). Baseline signals for SS and LS optodes are also shown at the bottom panels of Fig. 3. The green box emphasizes a portion where the Source SS signal resembles the LS signal while the yellow box emphasizes a portion where the Detector SS signal resembles the LS signal. These boxes illustrate the main hypothesis behind the double short separation method that the superficial interferences beneath the source and the detector may be different and that using two short separation measurements allows one to better capture the interference.

This procedure was repeated 30 times for each baseline measurement to create 30 simulated time courses with 30 different onset times to ensure robust averaged results. The duration of the synthetic response was 8 seconds as shown in Fig. 3. The resulting 1800 time courses (60 time courses × 30 simulated runs) were then band-pass filtered (0.01-1.25 Hz) and passed to the Kalman filter algorithm as depicted in Fig. 2. This algorithm was employed 3 times, using three different regressor cases: the SS measurement located close to the detector

(Det SS), the SS measurement located close to the source (Src SS) and both SS measurements simultaneously (Src&Det). To provide a comparison where no SS measurements are used, the HRF was also recovered using a standard GLM approach, using a set of cosine bases with a 64 s period cuto (Friston, 2000) to model the baseline physiology and the same temporal basis set used in the Kalman filter to model the HRF. Although simultaneous HbO and HbR estimation is possible (Diamond et al., 2006), the HbO and HbR responses were recovered independently in this work to prevent potential crosstalk introduced by noise in the regression (Strangman et al., 2003). For each SS-LS combination, the baseline Pearson R^2 correlation coefficient after adding the synthetic HRF to the LS channel was computed.

The quality of each recovered HRF was quantified using four different metrics: (1) the Pearson correlation coefficient R^2 between the true synthetic HRF and the recovered HRF, (2) the mean square error (MSE) between the true HRF and the recovered HRF, (3) the baseline noise defined by taking the standard deviation over the intervals -5 to 0 sec prior to the stimulus onset and (4) the inter-trial variability obtained by computing the standard deviation across individual trials and taking the mean of the obtained variability over the interval 0 to 12 sec following the stimulus onset.

The average for each of these four metrics across all the recovered HRFs for each specific regressor was computed and the results obtained were compared using two-tailed paired t-tests. As in our previous papers (Gagnon et al., 2011, 2012), we used a paired t-test to resolve for small systematic differences. For the Pearson R^2 metric, the average was taken after applying a Fisher transformation and the resulting average was then back transformed.

2.4. Experimental finger tapping

The functional data acquired during the finger tapping task were analyzed in the same way as above using the Kalman filter algorithm, but the HRFs were recovered from -5 to 18 sec after the stimulus onsets. Each of the four LS channels was analyzed using the three regressor cases derived from its closest SS measurements (Det SS, Src SS and Src&Det). The noise and the inter-trial variability metrics described above were also computed. The R^2 and the MSE metrics were not computed for the experimental finger tapping data since the true HRF is unknown.

3. Results

3.1. Baseline R^2 correlation results

The baseline R^2 coefficients between the SS and LS channel were computed and are shown in Table 1. The correlations computed for the simulations as well as for the experimental finger tapping are shown. For the simulations, the correlation was computed after the synthetic HRFs were added to the baseline LS trace and the evoked systemic artifacts were added to both the LS and SS traces. These correlations were calculated after all NIRS signals were bandpass filtered between 0.01 and 1.25 Hz to remove instrumental noise and drifts. As shown in Table 1, the baseline correlation was higher between the LS signal and the source SS signal than between the LS signal and the detector SS signal.

3.2. Simulation results

The metrics described in section 2.3 were computed over the 1800 recovered HRFs for each of the three regressor cases (Det SS, Src SS and Src&Det). To address how often the SS method improves the recovery of the HRF, we computed a likelihood ratio (as a percentage) which describes how often the SS method improved the recovery of the HRF in the 1800 traces of our simulations. The comparison was based on the performance obtained with the

standard GLM and the likelihood was computed individually for each regressor case and using each of the four metrics. These likelihoods are shown in Table 2. An improvement was identified as an increase for R^2, and as a decrease for MSE, Noise and inter-trial variability. Likelihoods were computed by taking the ratio of the number of recovered HRFs which meet these criteria and dividing by 1800, the total number of recovered HRFs, and converting to a percentage.

Table 2 illustrates that the likelihood of improvement is higher for HbO compared to HbR. This pattern is consistent regardless of the metric used to assess the performance of the regression. Using two SS measurements resulted in an improved HRF 96% of the time for HbO and 53% of the time for HbR (based on the MSE metric).

The recovered HRF averaged across all subjects, all channels, all trials and all repetitions are shown in Fig. 4 for each of the four recovery methods (3 regressors cases + GLM). The width of the traces indicates the standard deviation taken across all simulations (5 subjects, 3 runs, 4 channels, 30 trials, 30 repetitions). The true simulated HRF is illustrated by dotted lines.

The evoked systemic artifact is still present in the HbO response recovered with the GLM and this resulted in an overestimation of the HbO response when no SS regressor was applied. The removal of the evoked systemic artifact was improved progressively as the detector SS, the source SS and both the source and the detector SSs were applied

A quantitative comparison of the different regressor cases is shown in Fig. 5. The values of the four performance metrics described in section 2.3 were compared for the three different regressor cases as well as for the standard GLM without SS regression. A significant improvement in performance was observed for all metrics ($p<0.05$, two-tailed paired t-test) when two SSs were used compared to using a single SS measurement.

3.3. Experimental finger tapping results

Fig. 6 shows the HRFs recovered during the finger tapping task for each of the four recovery methods. Results are shown for a single run and for a single subject to illustrate the high quality of the recovery and the traces corresponding to the 18 individual trials are shown to illustrate the variability. The mean HRFs are also illustrated by a black dotted line in each case.

Quantitative comparisons of the noise and inter-trial variability were computed over the 15 runs (5 subjects, 3 runs each). Results are shown in the bar graphs of Fig. 7. A decrease in both noise and inter-trial variability ($p<0.05$, two-tailed paired t-test) was observed when two SS signals were used compared to a single SS. This trend was observed for both HbO and HbR.

3.4. Combined results

To illustrate quantitatively the gain obtained by using two SS measurements, the noise levels and the inter-trial variability in the recovered HRFs were compared explicitly for the four different recovery methods across both the simulations and the experimental finger tapping results. Values are shown in Table 3.

Across all simulation and experimental results, the noise level for HbO decreased on average from 6.6 μM when using the GLM to 4.6 and 4.3 μM when using the detector SS and the source SS respectively. This corresponds to a decrease of 31 and 35% respectively. When both SS signals are used, the noise further drops to 2.7 μM, a decrease of 59% when compared to the standard GLM. For HbR, the noise level dropped on average from 3.3 to

3.2 μM using the detector SS or the source SS. This corresponds to a decrease of 2.6%. When the two SSs are used, the noise further drops to 1.8 μM, a decease of 47% when compared to the standard GLM procedure.

The inter-trial variability for HbO went from 19.6 μM when using the GLM to 10.3 and 11.9 μM when using the detector SS and the source SS respectively. This corresponds to a decrease of 46 and 38% respectively. When both SS signals are used, the variability further drops to 5.4 μM, a decrease of 72% when compared to the GLM. For HbR, the variability went from 12.8 μM to 9.4 and 9.7 μM using the detector SS and the source SS respectively. This corresponds to a decrease of 27 and 25% respectively. When the two SSs are used, the inter-trial variability further drops to 3.0 μM, a decrease of 76% when compared to the GLM.

4. Discussion

4.1. Using two SS measurements is better than using only one

Our results show that using two SS measurements, one located close the source optode of the LS channel and one located close to the detector optode of the LS channel results in better performance of the SS method compared to when a single SS regressor is used. From our results in Table 3 (simulation and experimental), further improvements from 33% (Det: 30.5%, Src: 34.7%) to 59% in noise reduction and from 42% (Det: 46.0%, Src: 37.6%) to 72% in inter-trial variability were achieved for HbO. These values improved from 3% (Det: 2.6%, Src: 2.6%) to 47% for noise reduction and from 26% (Det: 26.9%, Src: 24.7%) to 76% for inter-trial variability for HbR. These improvements strongly motivate the incorporation of short separation measurements both at the source and at the detector optode of the LS channel.

The fact that two SSs perform better than a single SS is a consequence of the inhomogeneity of systemic physiology across the surface of the scalp. This inhomogeneity of the systemic physiology was described in our previous work (Gagnon et al., 2012). Because the two SS measurements are located 3 cm away from each other, they measure different superficial hemodynamic signals, which do not correlate exactly with one other. This is probably due to the inhomogeneous nature of the vascular network in the scalp.

Since the standard LS measurement constitutes an integratation of concentration changes throughout the volume traversed by the NIR light, the LS signal will contain systemic physiology that cannot entirely be described by a single SS signal, but will be better modelled by a linear combination of our two SS signals, as illustrated in Fig. 3. For this reason, using two SS measurements as regressor inputs to our Kalman filtering algorithm allows for improved recovery of the functional hemodynamic response signal of the brain

4.2. Source SS versus Detector SS

Because of the inherent symmetry of the measurement sensitivity between source and detector, a single SS measurement should perform identically whether it is placed close to the source optode or the detector optode of the LS measurement. In practice, small differences in performance can occur. As shown in Fig. 1, it was necessary to place an optical filter at the tip of the additional source to avoid saturation of the standard LS detector. In theory, the attenuation of the filter should be chosen such that the LS detector detects an equal amount of light coming from both sources. Because of the limited number of optical filter attenuations available, this condition is not always met. In our study, the attenuation of the filter selected (ND 2.00) was a little too high, resulting in a noisier signal and therefore a lower correlation between the SS signal close to the detector optode and the

LS signal, as shown in Table 1. This resulted in a better performance of the Src SS compared to the Det SS. Using a NIRS system allowing the intensity of the sources to be adjusted easily would solve this problem.

4.3. HbO vs HbR

The results in Table 2 show that the SS method is more likely to improve the recovery of the HRF for HbO than for HbR. Futhermore, the improvements obtained using the SS method were larger for HbO than for HbR. These results are in agreement with previous studies (Zhang et al., 2009; Gagnon et al., 2011).

While the SS method did not improve the HbR recovery in 47% of cases in our simulations (based on the MSE metric), the amplitude of the decreases in performance was very low compared to the amplitude of the increases in performance resulting in an overall improvement when results were averaged across all simulations ($p<0.05$, two-tailed paired t-test) as shown in Fig. 5. This result is consistent with our previous work (Gagnon et al., 2011) which reported no decrease in performance for HbR, though only averaged results were provided. The fact that the likelihood of improvement is lower for HbR should not prevent the use of the SS method for HbR since potential decreases in performance will not be meaningful compared to the potential benefits. We showed in our previous work (Gagnon et al., 2012) that a high improvement could be obtained for HbR as long as the baseline correlation between the LS and the SS was high. However, in practice, lower baseline correlations are obtained for HbR resulting in lower overall averaged performance. The reason for this lower baseline correlation is unclear. A potential explanation is that the interference mainly comes from the arteries, which contain mostly oxygenated blood (HbO). The HbR component of the arterial blood is comparatively much weaker (and therefore more noisy) which results in lower baseline correlation. Future investigation will be required to identify the underling physiological mechanism. Nevertheless, researchers can always predict the performance of the Kalman regression algorithm by computing the baseline correlation between the LS and the SS channels and thus decide whether this processing approach is the most appropriate.

4.4. Practical difficulties

Using SS measurements both at the source and at the detector presents two challenges. The first is the challenge of ensuring that the light levels match well the dynamic range of the photo-detector. As discussed in section 4.2, an optical filter must be placed at the tip of the additional source to overcome the low dynamical range and avoid detector saturation. The second difficulty is the high density of fibers required which makes the optical probe heavier and less flexible.

The results presented in this paper suggest that real benefits are obtained using two SS measurements compared to using a single one. These benefits are significant in cases where only a few trials can be performed such as in clinical studies (Haginoya et al., 2002; Buchheim et al., 2004; Wallois et al., 2010; Machado et al., 2010). However, in cases where several trials can be averaged, using a single SS detector located close to the source might be sufficient and less troublesome. Another example where two SS might be beneficial is when the NIRS signals are used to compute the cerebral metabolic rate of oxygen (CMRO2) (Huppert et al., 2009; Tak et al., 2010, 2011; Yucel et al., 2012) since higher levels of physiological noise could a ect the accuracy of the CMRO2 estimation.

4.5. Future directions

It has been recently shown that tomographic reconstruction can accurately remove superficial artifacts from NIRS data (Gregg et al., 2010). The researchers also compared the

performance of tomographic reconstruction with and without short separation signal regression where the short separation was regressed using a static linear minimum mean square estimator (LMMSE) as in (Saager and Berger, 2005; Saager et al., 2011). They concluded that each method improves the contrast-to-noise ratio when used alone, and that the two methods act synergistically, with greater improvements when used together. Since the Kalman filter used in the present study has been shown to perform better than the static estimator (Gagnon et al., 2011) used by Gregg et al (2010), it would be interesting in future work to investigate (1) how the Kalman filter compared with tomographic reconstruction alone, and (2) how much is gained when used together with tomographic reconstruction.

5. Conclusion

This work has demonstrated that using two short separation measurements, one located close to the source optode and one located close to the detector optode further improves the performance of the Kalman short separation regression method compared to using a single short separation measurement. Using both simulated and experimental functional activation, reductions of 59% in noise level and 72% in inter-trial variability were obtained for HbO and reductions of 47% in baseline noise level and 76% in inter-trial variability were obtained for HbR compared to a standard GLM approach. Our work emphasizes the importance of designing multi-distance NIRS probes that incorporate short separation measurements at both the source and the detector optode of the standard 3 cm NIRS channels.

Acknowledgments

This work was supported by NIH grants P41-RR14075, R01-EB006385, R01-EB000790 and R90-DA023427. L. Gagnon was supported by the Advanced Multimodal NeuroImaging Training Program at MIT.

References

Boas D, Dale AM, Franceschini MA. Diffuse optical imaging of brain activation: Approaches to optimizing image sensitivity, resolution and accuracy. NeuroImage. 2004; 23:S275–S288. [PubMed: 15501097]

Brainard DH. The psychophysics toolbox. Spatial Vision. 1997; 10:433–436. [PubMed: 9176952]

Buchheim K, Obrig H, Pannwitz W, Muller A, Heekeren H, Villringer A, Meierkord H. Decrease in haemoglobin oxygenation during absence seizures in adult humans. Neuroscience Letters. 2004; 354:119–122. [PubMed: 14698453]

Deply DT, Cope M, van der Zee P, Arridge S, Wray S, Wyatt J. Estimation of optical pathlength through tissue from direct time of flight measurement. Phys. Med. Biol. 1988; 33:1433–1442. [PubMed: 3237772]

Diamond S, Huppert TJ, Kolehmainen V, Franceschini MA, Kaipo JP, Arridge SR, Boas DA. Dynamic physiological modeling for functional diffuse optical tomography. NeuroImage. 2006; 30:88–101. [PubMed: 16242967]

Ferrari M, Caresima V. A brief review on the history of human functional near-infrared spectroscopy (fNIRS) development and fields of application. NeuroImage. 2012

Friston K. Nonlinear responses in fMRI: The balloon model, volterra kernels, and other hemodynamics. NeuroImage. 2000; 12(4):466–477. [PubMed: 10988040]

Gagnon L, Cooper RJ, Yücel MA, Perdue KL, Greve DN, Boas DA. Short separation channel location impacts the performance of short channel regression in NIRS. NeuroImage. 2012; 59(3):2518–2528. [PubMed: 21945793]

Gagnon L, Perdue K, Greve DN, Goldenholz D, Kaskhedikar G, Boas DA. Improved recovery of the hemodynamic response in diffuse optical imaging using short optode separations and state-space modeling. NeuroImage. 2011; 56(3):1362–1371. [PubMed: 21385616]

Gelb, A. Applied Optimal Estimation. MIT Press; 1974.

Gregg NM, White BR, Zeff BW, Berger AJ, Culver JP. Brain specificity of diffuse optical imaging: improvements from superficial signal regression and tomography. Font. in Neuroenergetics. 2010; 2(14):1–8.

Haginoya K, Munakata M, Kato R, Yokoyama H, Ishizuka M, Iinuma K. Ictal cerebral haemodynamics of chilhood epilespsy measured with near-infrared spectroscopy. Brain. 2002; 125:1960–1971. [PubMed: 12183342]

Haykin, S. Kalman filtering and neural Networks. John Wiley & Sons; New York: 2001.

Hoshi Y. Functional near-infrared spectroscopy: current status and future prospects. J. Biomed. Opt. 2007; 12(6):062106. [PubMed: 18163809]

Huppert T, Hoge R, Dale AM, Franceschini M, Boas D. Quantitative spatial comparison of diffuse optical imaging with blood oxygen level-dependent and arterial spin labeling-based functional magnetic resonance imaging. J. Biomed. Opt. 2006a; 11(6):064018. [PubMed: 17212541]

Huppert T, Hoge R, Diamond S, Franceschini M, Boas D. A temporal comparison of BOLD, ASL, and NIRS hemodynamic responses to motor stimuli in adult humans. NeuroImage. 2006b; 29:368–382. [PubMed: 16303317]

Huppert TJ, Allen MS, Diamond SG, Boas DA. Estimating cerebral oxygen metabolism from fmri with a dynamic multicompartment windkessel model. Hum. Brain Mapp. 2009; 30(5):1548–1567. [PubMed: 18649348]

Kalman RE. A new approach to linear filtering and prediction problems. Journal of Basic Engineering. 1960; 82:35–45. Series D.

Kirilina E, Jelzow A, Heine A, Niessing M, Wabritz H, Bruehl R, Ittermann B, Jacobs AM, Tachtsidis I. The physiological origin of task-evoked systemic artefacts in functional near infrared spectroscopy. NeuroImage. 2011; 61:70–81. [PubMed: 22426347]

Lloyd-Fox S, Blasi A, Elwell CE. Illuminating the developing brain: The past, present and future of functional near infrared spectroscopy. Neuroscience & Biobehavioral Reviews. 2010; 34:269–284. [PubMed: 19632270]

Machado A, Lina J-M, Tremblay J, Lassonde M, Nguyen DK, Lesage F, Grova C. Detection of hemodynamic responses to epileptic activity using simultaneous electro-encephalography (EEG)/ near infra red spectroscopy (NIRS) acquisitions. NeuroImage. 2010; 56(1):114–125. [PubMed: 21168514]

Obrig Y, Villringer A. Beyond the visible: imaging the human brain with light. J. Cereb. Blood Flow Metab. 2003; 23:1–18. [PubMed: 12500086]

Rauch HE, Tung F, Striebel CT. Maximum likelihood estimates of linear dynamic systems. AIAA Journal. 1965; 3(8):1445–1450.

Saager RB, Berger AJ. Direct characterization and removal of interfering absorption trends in two-layer turbid media. J. Opt. Soc. Am. A. 2005; 22(9):1874–1882.

Saager RB, Telleri NL, Berger AJ. Two-detector corrected near infrared spectroscopy (C-NIRS) detects hemodynamic activation responses more robustly than single-detector NIRS. NeuroImage. 2011; 55(4):1679–1685. [PubMed: 21256223]

Strangman G, Franceschini MA, Boas DA. Factors affecting the accuracy of near-infrared spectroscopy concentration calculations for focal changes in oxygenation parameters. NeuroImage. 2003; 18:865–879. [PubMed: 12725763]

Tak S, Jang J, Lee K, Jeong Y, Ye JC. Quantification of CMRO2 without hypercapnia using simultaneous near-infrared spectroscopy and fMRI measurements. Phy. Med. Biol. 2010; 55:3249–3269.

Tak S, Yoon SJ, Jang J, Yoo K, Jeong Y, Ye JC. Quantitative analysis of hemodynamic and metabolic changes in subcortical vascular dementia using simultaneous near-infrared spectroscopy and fMRI measurements. NeuroImage. 2011; 55:176–184. [PubMed: 21094685]

Takahashi T, Takikawa Y, Kawagoe R, Shibuya S, Iwano T, Kitazawa S. nfluence of skin blood flow on near-infrared spectroscopy signals measured on the forehead during a verbal fluency task. NeuroImage. 2011; 57:991–1002. [PubMed: 21600294]

Umeyama S, Yamada T. Monte carlo study of global interference cancellation by multidistance measurement of near-infrared spectroscopy. J. Biomed. Opt. 2009; 14(6):064025. [PubMed: 20059263]

Wallois F, Patil A, Heberle C, Grebe R. EEG-NIRS in epilepsy in children and neonates. Clinical Neurophysiology. 2010; 40:281–292. [PubMed: 21093799]

Yamada T, Umeyama S, Matsuda K. Multidistance probe arrangement to eliminate artifacts in functional near-infrared spectroscopy. J. Biomed. Opt. 2009; 16(4):06434.

Yucel MA, Huppert TJ, Boas DA, Gagnon L. Calibrating the BOLD signal during a motor task using an extended fusion model incorporating DOT, BOLD and ASL data. NeuroImage. 2012; 61:1268–1276. [PubMed: 22546318]

Zhang Q, Brown EN, Strangman GE. Adaptative filtering for global interference cancellation and real-time recovery of evoked brain activity: a Monte Carlo simulation study. J. of Biomed. Opt. 2007; 12(4):044014. [PubMed: 17867818]

Zhang Q, Strangman G, Ganis G. Adaptive filtering to reduce global interference in non-invasive nirs measures of brain activation: How well and when does it work? NeuroImage. 2009; 45:788–794. [PubMed: 19166945]

Research Highlights

- Two short separation channels is better than a single short separation
- Reductions of 59% in noise and 72% in inter-trial variability achieved for HbO
- Reduction of 47% in noise level and 76% in inter-trial variability for HbR
- Improvements are significant enough to justify the practical challenges

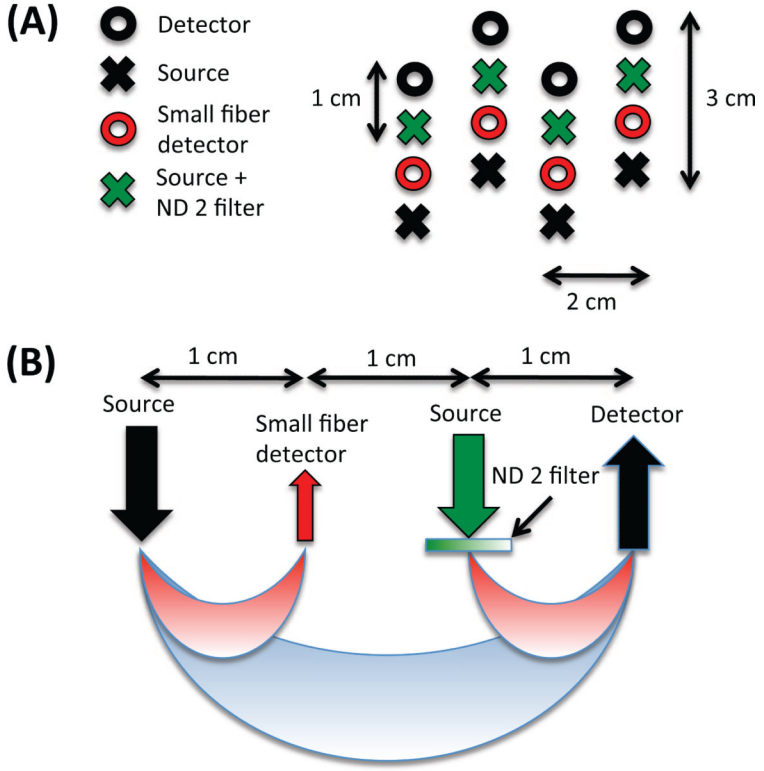

Figure 1.
NIRS probe. (A) Geometry (B) Sensitivity In order to avoid detector saturation, 200 μm-core fibers were used for the SS detectors (shown in red) and a piece of optical filter (Kodak WRATTEN ND 2.00) was glued at the tips of standard NIRS fibers (shown in green) for the additional sources of the SS measurements.

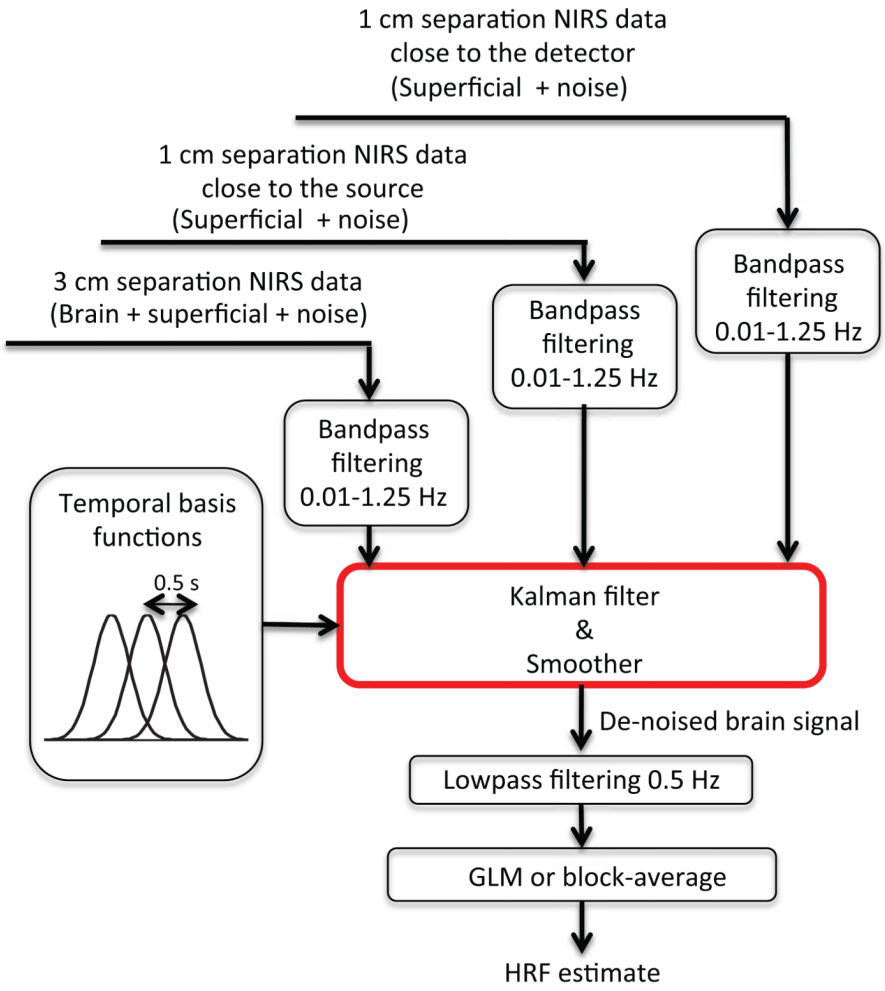

Figure 2.
Overview of the algorithm for data analysis. Both the SS and LS measurements were bandpass filtered at 0.01-1.25 Hz and then used simultaneoulsy as regressors in the Kalman filter. A set of temporal basis functions was used to lower the dimensionality of the problem. The output of the Kalman filter was further low pass filtered at 0.5 Hz to remove any cardiac fluctuations potentially present in the time course and the final estimate of the hemodynamic response was obtained by applying a standard General Linear Model (GLM) procedure.

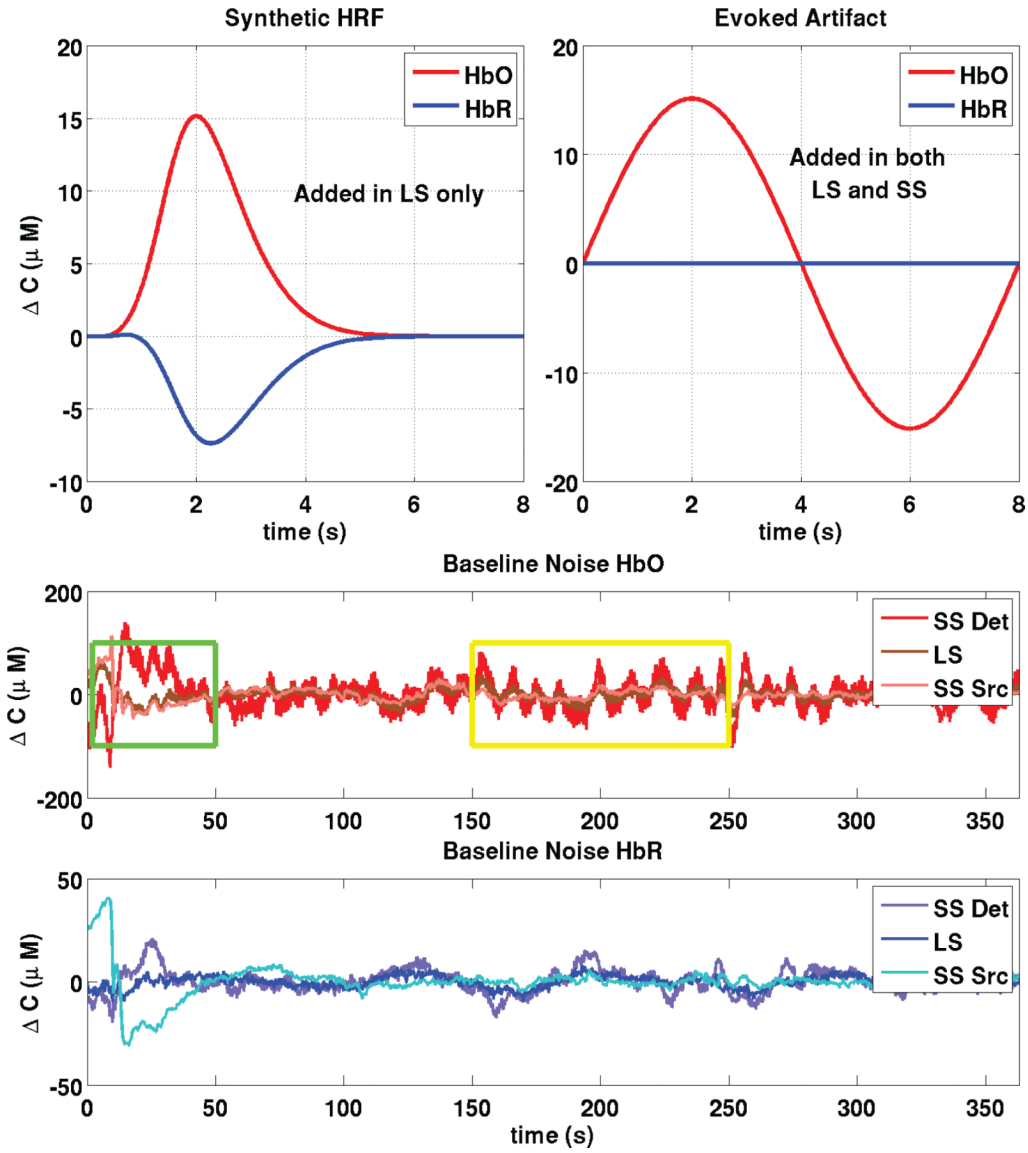

Figure 3.

Construction of synthetic data. Thirty individual evoked responses were added over all 60 LS baseline measurements (5 subjects × 3 runs × 4 LS channels) at random onset times with an inter-stimulus interval taken randomly from a uniform distribution (12-30 sec). We also added an evoked systemic artifact to the HbO signals (LS and SS) that was phase-locked with the stimulus onset. The green box emphasizes a portion of the baseline signal where the Source SS signal resembles the LS signal while the yellow box emphasizes a portion where the Detector SS signal resembles the LS signal.

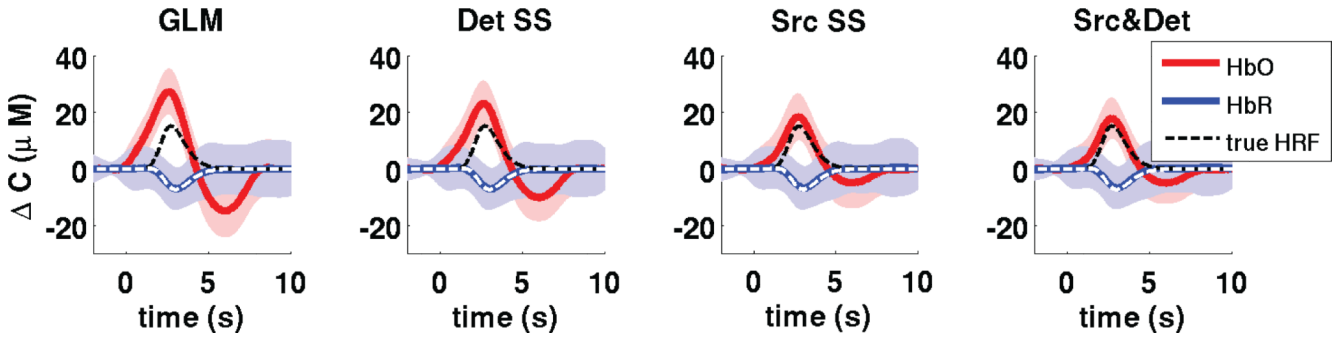

Figure 4.

Averaged recovered HRF across all simulations. The width of the traces represent uncertainty given by one standard deviation taken across all simulations (5 subjects, 3 runs, 4 channels, 30 trials, 30 noise instances). The true simulated HRF is shown with dotted lines in each case.

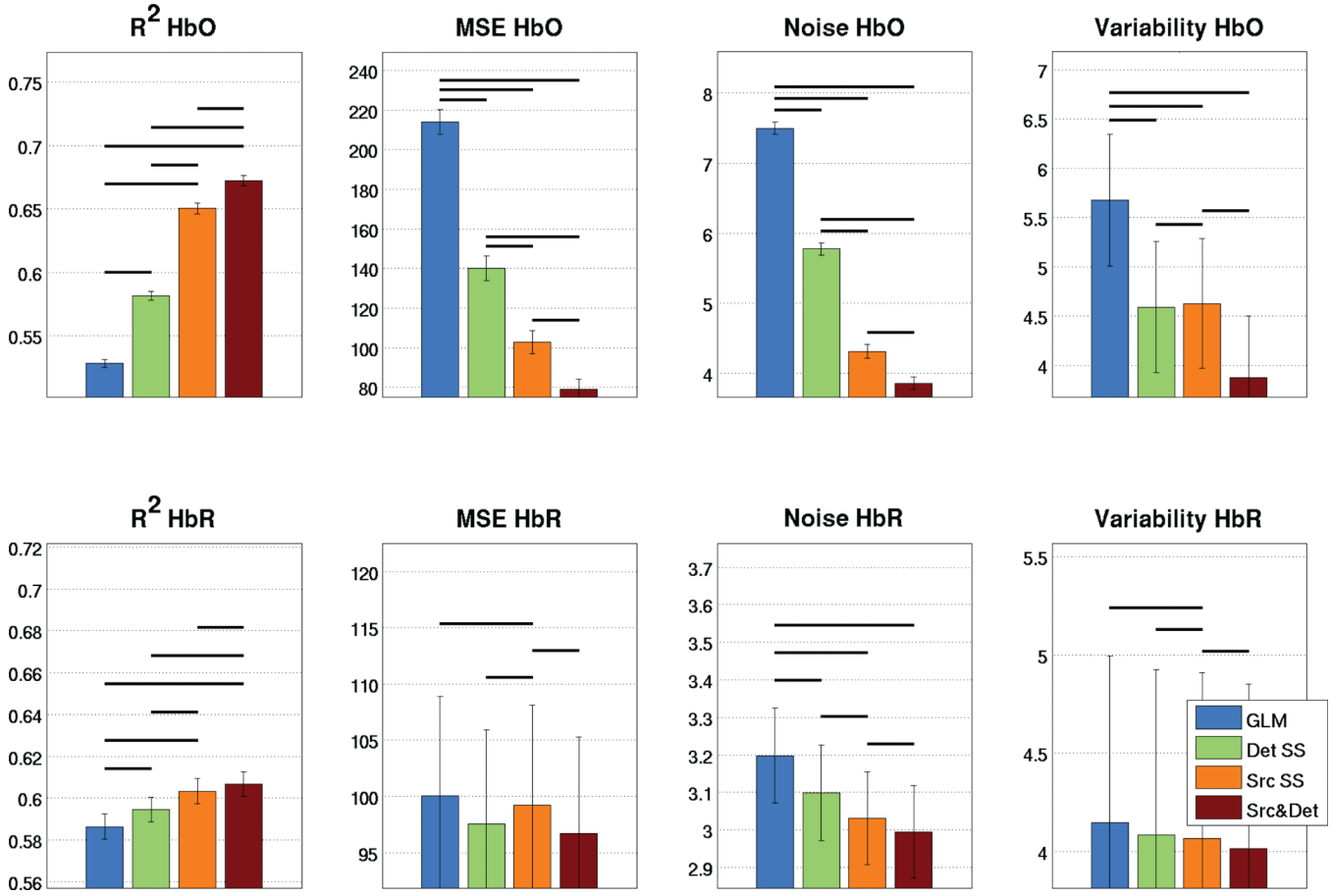

Figure 5.

Quantitative analysis of the 1800 simulations. Bars represent the mean taken across all simulated HRFs and error bars represent the standard error on the mean. Statistical significance at the $p<0.05$ level (two-tailed paired t-test) is illustrated by black lines over the bars.

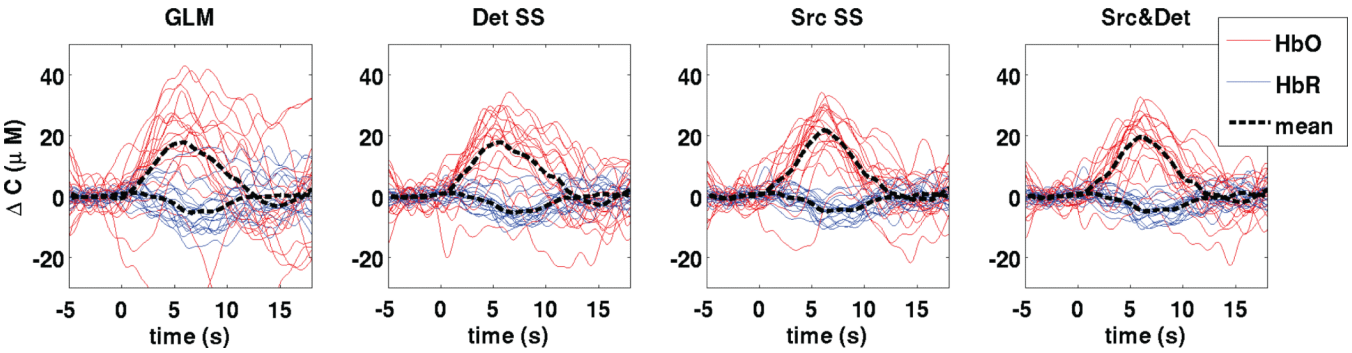

Figure 6.

HRFs recovered during the experimental finger tapping for a representative subject for a single run. The HRFs for each of the 18 individual trials are shown in red for HbO and blue for HbR. The mean HRF taken across the 18 trials is shown by a black dotted line.

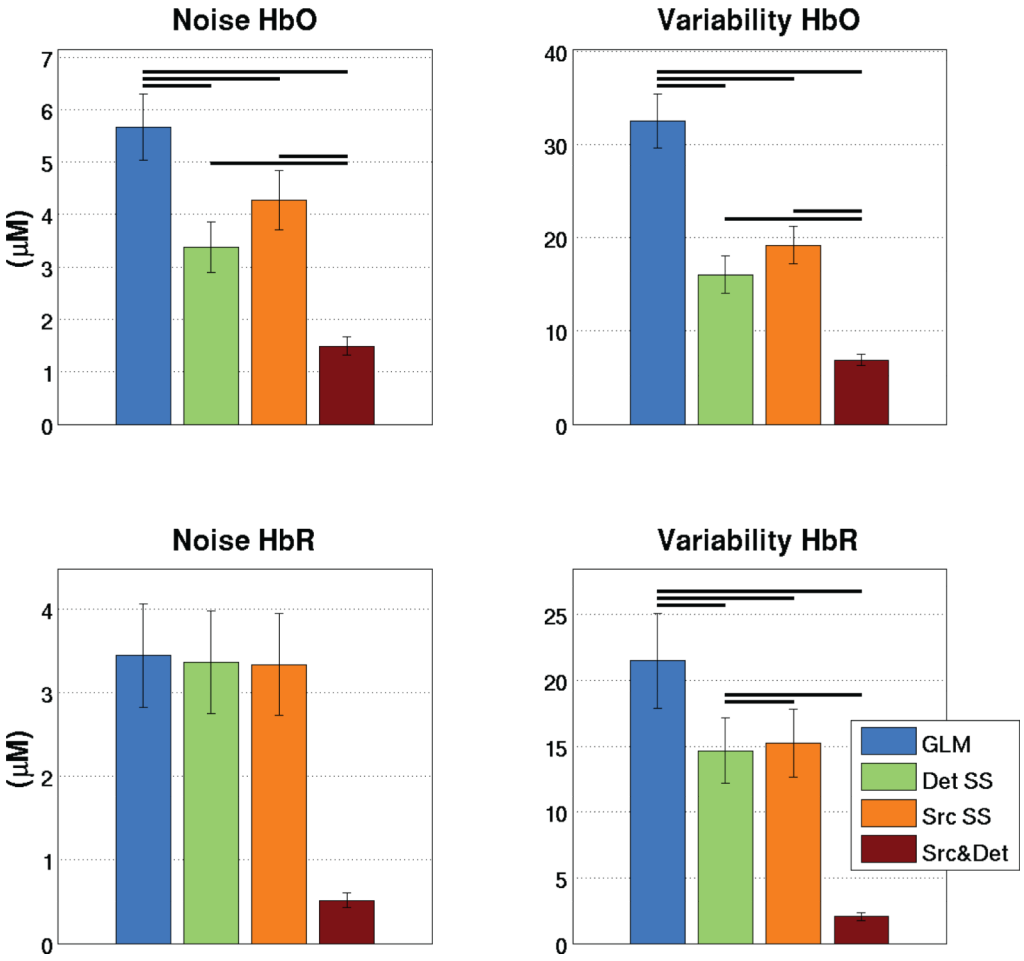

Figure 7.

Quantitative analysis of the experimental finger tapping. Bars represent the mean taken across all runs and error bars represent the standard error on the mean. Statistical significance at the $p<0.05$ level (two-tailed paired t-test) is illustrated by black lines over the bars.

Table 1

Baseline R^2 correlation between LS and SS signals.

Optode	Sim HbO	Exp HbO	Sim HbR	Exp HbR
Src SS	0.39	0.38	0.24	0.13
Det SS	0.28	0.29	0.08	0.04

Table 2

Likelihood of improving the recovery of the HRF with the SS method compared to the standard GLM method. The likelihoods were computed by comparing the HRFs recovered over the 1800 simulated time courses of our simulations.

	Det SS (%)	Src SS (%)	Src&Det (%)
HbO			
R^2	77	83	85
MSE	89	94	96
Noise	88	92	95
Variability	95	88	95
HbR			
R^2	47	50	51
MSE	49	52	53
Noise	52	54	55
Variability	47	50	48

Table 3

Comparison of the level of noise in the recovered HRF for different regressors. Combined (simulations + experimental finger tapping) results are shown.

Method	Noise (μM)	Comparison with GLM (%)	Comparison with Det SS (%)	Comparison with Src SS (%)
Noise HbO				
GLM	6.6			
Det SS	4.6	-30.5		
Src SS	4.3	-34.7		
Src&Det	2.7	-59.3	-41.5	-37.7
Noise HbR				
GLM	3 3			
Det SS	3.2	-2.6		
Src SS	3.2	-2.6		
Src&Det	1.8	-47.1	-45.7	-44.9
Variability HbO				
GLM	19.1			
Det SS	10.3	-46.0		
Src SS	11.9	-37.6		
Src&Det	5.4	-71.9	-47.9	-54.9
Variability HbR				
GLM	12.8			
Det SS	9.4	-26.9		
Src SS	9.7	-24.7		
Src&Det	3.0	-76.4	-67.6	-68.6